Auroral clutter observations with a three-dimensional over-the-horizon radar

Ryan J. Riddolls
Defence R&D Canada - Ottawa
3701 Carling Avenue
Ottawa, Ontario, Canada K2G 0R3
Email: ryan.riddolls@drdc-rddc.gc.ca

***Abstract*— An Over-The-Horizon Radar (OTHR) has been deployed near Ottawa, Canada. The radar is aimed northward and collects auroral echoes through line-of-sight propagation and ground echoes from beyond the horizon through ionospheric reflection. These echoes have been resolved in the three spatial dimensions of range, azimuth, and elevation, as well as in the temporal dimension of Doppler. It is shown that the three-dimensional spatial resolving capability is useful for separating the auroral and ground echo components.**

I. Introduction

High-latitude Over-The-Horizon Radar (OTHR) systems must contend with clutter arising from Bragg scatter produced by plasma density irregularities in the Earth's auroral zone [1]. Successful operations might require the auroral clutter to be filtered in one or more of the radar observable dimensions, consisting of range, azimuth, elevation, and Doppler. Early OTHR systems [2] were essentially one-dimensional in the sense of having one spatial dimension (range) in addition to the dimension of time (Doppler). Current-generation systems [3] use wide-aperture receive arrays, which provide spatial resolution in azimuth in addition to range. Next-generation systems may use two-dimensional arrays on transmit and/or receive [4] to provide three dimensions of spatial resolution, namely range, azimuth, and elevation.

Recent articles [5], [6] have suggested that the localization of auroral echoes in Doppler, range, azimuth, and elevation, could be compromised by signal scintillation arising from radio wave propagation in a drifting plasma media with spatial index of refraction fluctuations. The scintillation can be thought of as a point-spread function (PSF) that convolves with the clutter source distribution to provide the observed three-dimensional clutter distribution. The PSF particularly impacts the azimuth and elevation dimensions, as these dimensions depend on the spatial structure of the signal phase, which is subject to scintillation during the ionospheric propagation.

This paper presents the following material. A geometric optics theory of propagation in plasma irregularities is provided in Section II, which is a simplified version of [7]. In Section III, experimental observations from a Canadian three-dimensional OTHR system are shown and interpreted in terms of the theory. The experiments use the OTHR system described in [8] and also use methods described in [9] to estimate the azimuth and elevation spectra.

II. Theory

Signals propagating in media with spatial refractive index fluctuations experience phase scintillation. The phase is

$$\phi = \int_S k(\mathbf{r})\, ds, \tag{1}$$

where S is the radar signal ray trajectory, $k(\mathbf{r})$ is the radar signal wavenumber, $\mathbf{r}$ is a location on S, and ds is an element of arc length. For low-elevation radar beams, we approximate S as a straight line in the x direction (north), with y west and z up (see [6] for more complicated trajectories). Let us consider a first-order Taylor series perturbation of $k(\mathbf{r})$ with respect to plasma density n, so that the phase perturbation is

$$\phi_1 = \int_S n_1(x) \frac{\partial k}{\partial n}\, dx, \tag{2}$$

where n_1 is the plasma density perturbation. For simplicity, we consider unmagnetized plasma with dispersion relation

$$\omega^2 = c^2 k^2 + \frac{e^2 n}{\epsilon_0 m_e}, \tag{3}$$

where ω is the frequency, c is the speed of light, e is the charge on an electron, ϵ_0 is the permittivity of free space, and m_e is the mass of an electron. Using (3) in (2), we find

$$\phi_1 = -r_e \lambda \int_S n_1(x)\, dx, \tag{4}$$

where $r_e = e^2/(4\pi\epsilon_0 m_e c^2) = 2.8 \times 10^{-15}$ m is the classical electron radius, and λ is the radar wavelength in the plasma. The spatial autocorrelation of ϕ_1 in the horizontal plane is

$$R_{\phi_1}(X, Y) = (r_e \lambda)^2 \iint_S R_{n_1}(X + x - x', Y)\, dx\, dx', \tag{5}$$

where R_{n_1} is the autocorrelation function of the plasma density perturbation. After Fourier transforms we have

$$S_{\phi_1}(\kappa_x, \kappa_y) = (r_e \lambda)^2 S_{n_1}(\kappa_x, \kappa_y) \iint_S e^{i\kappa_x (x - x')}\, dx\, dx' \tag{6}$$

$$= (L r_e \lambda)^2 \operatorname{sinc}^2(\kappa_x L/2)\, S_{n_1}(\kappa_x, \kappa_y), \tag{7}$$

where L is the total distance travelled in the plasma and $\operatorname{sinc}(x) = \sin(x)/x$. At high latitudes, we approximate the magnetic field as vertical, so that the plasma organizes itself such that S_{n_1} is rotationally symmetric around a vertical

axis. For a two-dimensional turbulent plasma, the Kolmogorov turbulence spectrum varies as $\kappa^{-8/3}$, approximated as κ^{-3} [5]:

$$S_{n_1}(\kappa_x,\kappa_y) = \frac{2\pi\kappa_0 \left\langle n_1^2\right\rangle}{(\kappa_0^2+\kappa_x^2+\kappa_y^2)^{3/2}}, \tag{8}$$

where κ_0 is the inverse scale length of the largest turbulent eddies. The spectrum is normalized as follows:

$$\left\langle n_1^2\right\rangle = \frac{1}{(2\pi)^2}\int_{-\infty}^{\infty}\int_{-\infty}^{\infty} S_{n_1}(\kappa_x,\kappa_y)\,d\kappa_x\,d\kappa_y. \tag{9}$$

We insert (8) in (7) and take inverse Fourier transforms:

$$R_{\phi_1}(X,Y) = \frac{\kappa_0(Lr_e\lambda)^2\left\langle n_1^2\right\rangle}{2\pi} \times\int_{-\infty}^{\infty}\int_{-\infty}^{\infty}\frac{\mathrm{sinc}^2(\kappa_x L/2)\,e^{i\kappa_x X+i\kappa_y Y}d\kappa_x d\kappa_y}{(\kappa_0^2+\kappa_x^2+\kappa_y^2)^{3/2}}. \tag{10}$$

We recall the identity

$$\frac{2|u|K_1(a|u|)}{a} = \int_{-\infty}^{\infty}\frac{e^{iux}\,dx}{(a^2+x^2)^{3/2}}, \tag{11}$$

where K_1 is the modified Bessel function of the second kind. By using (11) we find

$$R_{\phi_1}(X,Y) = \frac{\kappa_0(Lr_e\lambda)^2\left\langle n_1^2\right\rangle}{\pi} \times\int_{-\infty}^{\infty}\mathrm{sinc}^2(\kappa_x L/2)\frac{|Y|K_1\left[(\kappa_0^2+\kappa_x^2)^{1/2}|Y|\right]}{(\kappa_0^2+\kappa_x^2)^{1/2}}e^{i\kappa_x X}d\kappa_x. \tag{12}$$

Under the condition $5\times10^5\ \mathrm{m}\approx L\gg\kappa_0^{-1}\approx10^4\ \mathrm{m}$, the factor $\mathrm{sinc}^2(\kappa_x L/2)$ acts as a Dirac delta function with respect to factors of $(\kappa_0^2+\kappa_x^2)^{1/2}$. Hence

$$R_{\phi_1}(X,Y) = 2(Lr_e\lambda)^2\left\langle n_1^2\right\rangle|Y|K_1(\kappa_0|Y|) \tag{13}$$

$$\times\frac{1}{2\pi}\int_{-\infty}^{\infty}\mathrm{sinc}^2(\kappa_x L/2)e^{i\kappa_x X}\,d\kappa_x. \tag{14}$$

We note the Fourier transform relationship

$$\frac{1}{2\pi}\int_{-\infty}^{\infty}\mathrm{sinc}^2(\kappa_x L/2)e^{i\kappa_x X}\,d\kappa_x = \frac{1}{L}\mathrm{tri}\,(X/L)\,, \tag{15}$$

where $\mathrm{tri}(\mathrm{x}) = (1-|x|)\mu(1-|x|)$ is the triangle function, and $\mu(x)$ is the step function. The final form of the correlation is

$$R_{\phi_1}(X,Y) = 2L(r_e\lambda)^2\left\langle n_1^2\right\rangle\ \mathrm{tri}\,(X/L)\ |Y|K_1(\kappa_0|Y|). \tag{16}$$

This is the same general form as was found in [7], but with differing constants due to the simplified trajectory. Here, the mean-square value of ϕ_1 is

$$\left\langle\phi_1^2\right\rangle = R_{\phi_1}(0,0) = \frac{2L(r_e\lambda)^2\left\langle n_1^2\right\rangle}{\kappa_0}. \tag{17}$$

As an example, let us consider $L=500$ km, $\lambda=30$ m, and $\left\langle n_1^2\right\rangle = 10^{18}\ \mathrm{m}^{-6}$, which represents 1-percent density fluctuations of a peak ionosphere density of $10^{11}\ \mathrm{m}^{-3}$. This gives us a root-mean-square phase fluctuation $\sqrt{\left\langle\phi_1^2\right\rangle}$ on the order of 10 radians. The complex amplitude of the phase-scintillated radar signal is given by $A = e^{i\phi_1}$. The complex amplitude autocorrelation is related to the phase autocorrelation by [10]:

$$R_A(X,Y) = \left\langle e^{-i\phi_1(x,y)}e^{i\phi_1(x+X,y+Y)}\right\rangle = e^{R_{\phi_1}(X,Y)-\left\langle\phi_1^2\right\rangle}. \tag{18}$$

The complex amplitude autocorrelation function is thus

$$R_A(X,Y) = e^{-\left\langle\phi_1^2\right\rangle[1-\mathrm{tri}(X/L)\kappa_0|Y|K_1(\kappa_0|Y|)]}. \tag{19}$$

The angular PSF is the Fourier transform of the autocorrelation function. $R_A(X,Y)$ is not a separable function X and Y, so we consider individually the marginal spectra $S_A(\kappa_x)$ and $S_A(\kappa_y)$. For $S_A(\kappa_x)$, we approximate $R_A(X,0)$ as

$$R_A(X,0)\approx e^{-\left\langle\phi_1^2\right\rangle|X|/L}, \tag{20}$$

such that the approximation is good where the function is non-negligible. The marginal spectrum in the x direction is the well-known Fourier transform:

$$S_A(\kappa_x) = \frac{2\left\langle\phi_1^2\right\rangle/L}{\left(\left\langle\phi_1^2\right\rangle/L\right)^2+\kappa_x^2}. \tag{21}$$

This spectrum is unit area with two-sided width of $\Delta\kappa_x = 2\left\langle\phi_1^2\right\rangle/L$, and second-order sidelobe rolloff. At 10 MHz, the radar radial wavenumber is $k=0.21\ \mathrm{m}^{-1}$, so for a beam elevation of $\theta=10$ degrees, the achievable elevation resolution is $\Delta\theta = \Delta\kappa_x/(k\sin\theta)\approx 0.6$ degrees. Thus the mainlobe is narrow, but the sidelobe rolloff is slow. At a separation of 10 degrees from the mainlobe (30 times the one-sided mainlobe width), the sidelobes are at best 30 dB down. Turning to the case of $S_A(\kappa_y)$, we note the small-argument expansion [11]

$$zK_1(z)\approx 1+(z^2/2)\log(z/2). \tag{22}$$

This allows one to approximate $R_A(0,Y)$ as

$$R_A(0,Y)\approx e^{\left\langle\phi_1^2\right\rangle(\kappa_0|Y|)^2\log(\kappa_0|Y|/2)/2}, \tag{23}$$

such that the approximation is good where the function is non-negligible. Disregarding the slowly-varying (and near-unity) logarithm factor, we estimate the one-sided width of the above function as approximately $(\kappa_0\sqrt{\left\langle\phi_1^2\right\rangle})^{-1}$, and thus the one-sided width of its Fourier transform is approximately $\kappa_0\sqrt{\left\langle\phi_1^2\right\rangle}$. Furthermore, by taking derivatives of the above expression, one can show that only the first two derivatives are continuous at the origin, which indicates a fourth-order sidelobe rolloff. The Fourier transform is thus approximately

$$S_A(\kappa_y) = \frac{2\kappa_0^3\left\langle\phi_1^2\right\rangle^{3/2}}{(\kappa_0^2\left\langle\phi_1^2\right\rangle+\kappa_y^2)^2}, \tag{24}$$

where the spectrum has been normalized to unit area. The (two-sided) width of the transform is therefore approximately $\Delta\kappa_y = 2\times10^{-3}\ \mathrm{m}^{-1}$. At 10 MHz, the radar radial wavenumber is $k=0.21\ \mathrm{m}^{-1}$, so at boresight the achievable azimuth resolution is $\Delta\varphi = \Delta\kappa_y/k\approx 0.6$ degree, which is similar to the elevation resolution. However, the sidelobes have fourth-order as opposed to second-order rolloff, meaning that at a separation of 10 degrees, the sidelobes can be as much as 60 dB down. This means that the cancellation of auroral clutter may be easier in azimuth than in elevation.

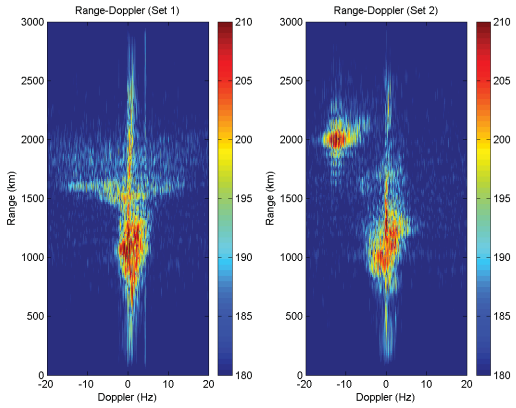

Fig. 1. Range-Doppler maps of Set 1 and Set 2.

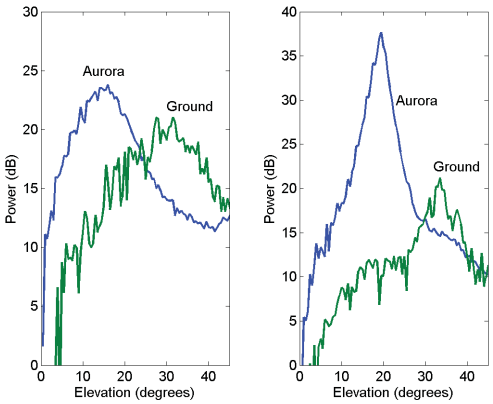

Fig. 2. Elevation distributions of Set 1 and Set 2.

III. Experiment

Two data sets will be presented in this section. The sets were collected on 13 Sep 2013 at 0637 and 0844 UTC. Figure 1 shows range-Doppler processed data for Set 1 and Set 2. In both sets we see ground clutter at 0 Hz extending through much of the unambiguous range, with Doppler-spreading of the ground clutter evident between about 800 km and 1,300 km in range. In Set 1, auroral clutter is evident between about 1,400 km and 1,900 km in range, and spread over about ± 15 Hz in Doppler. In Set 2, the auroral clutter is located between about 1,800 km and 2,200 km in range, and spread between about -19 Hz and -7 Hz in Doppler. These data sets show that the range-Doppler locations and spreadings of the auroral clutter are variable with time, and a clutter rejection scheme must be flexible to accommodate these variations. Furthermore, the auroral clutter in Set 1 is clearly co-located in range and Doppler with ground clutter, so the ground scene could be masked by the auroral clutter. In Set 2, the auroral clutter is clearly separated from ground clutter in Doppler, although the auroral clutter still occurs at the same range as the ground clutter. In this case, the illuminated ground scene would be masked if elements of the scene produced Doppler shifts in the Doppler extent occupied by the auroral clutter.

Figure 2 shows elevation processed data for Set 1 and Set 2. To create these plots, data were selected from the range-Doppler plots of Figure 1 to represent either ground clutter or auroral clutter. For both data sets, we focused attention on the range interval of 1,500 km to 2,250 km. Within that range interval, the Doppler interval of -0.5 Hz to 0.5 Hz was selected to represent ground clutter and the interval of -20 Hz to -0.5 Hz was selected to represent auroral clutter. Elevation estimates were produced following the method of [9]. For Set 1 in Figure 2 the green trace shows the ground clutter and the blue trace shown the auroral clutter. The distributions are separated by about 15 degrees. To resolve this separation at frequencies down to 5 MHz, one needs a vertical aperture of about 250 m, which at an elevation of 15 degrees corresponds to a requirement for a ground-based 1-km endfire array.

In Set 2, the separation between the ground and auroral clutter has shrunk to about 10 degrees, but has moved up about 5 degrees in elevation. To obtain a resolution of 10 degrees at frequencies down to 5 MHz, one requires a vertical aperture of about 350 m, which at an elevation of 20 degrees corresponds again to a requirement for a ground-based 1-km endfire array. Also to be noted in these data sets are the slow sidelobe rolloffs in elevation suggested by the PSF from the theory, where we calculated rolloffs no better than 30 dB for a 10-degree separation in elevation from the auroral clutter echo. In the data sets, the rolloff appears to be bounded by the rate of 30 dB for a 10-degree separation, especially in Set 2. Thus one would likely need elevation processing on both transmit and receive if one wanted to separate ground and auroral modes purely in elevation.

Figure 3 shows range-azimuth processed data for Set 1 and Set 2. One must bear in mind that the response in the azimuth direction is somewhat impacted by the azimuthal response of the antennas, which tends to roll off outside ± 30 degrees azimuth. With this in mind, we turn to Set 1, where we see that the ground echo occupies a fairly large azimuth extent of -40 to about 70 degrees, whereas the auroral clutter modes are more localized in azimuth, with the two auroral modes being localized to -30 to 30 degrees and -10 to 40 degrees, respectively. We found earlier that the PSF is well-localized in azimuth (estimated as up to 60 dB rolloff at 10-degree offset) so the slow rolloffs that are observed in these images are likely due to the clutter distribution in azimuth as opposed to the PSF. This is not surprising, since the bottomside ionosphere has a large horizontal extent relative to the vertical extent, and thus one might expect graceful tapering of the distributions in azimuth. Nevertheless, the auroral clutter is more confined in azimuth than the ground clutter, suggesting an opportunity to resolve the auroral clutter from the ground clutter.

In Set 2, we see an even more localized auroral clutter mode, occupying the azimuth extent -50 to -10 degrees, leaving positive azimuth clear. It should be noted, however, that the blue horizontal bar seen at 2,000-km range is likely an artifact of the azimuth estimation technique [9]. The angle estimates

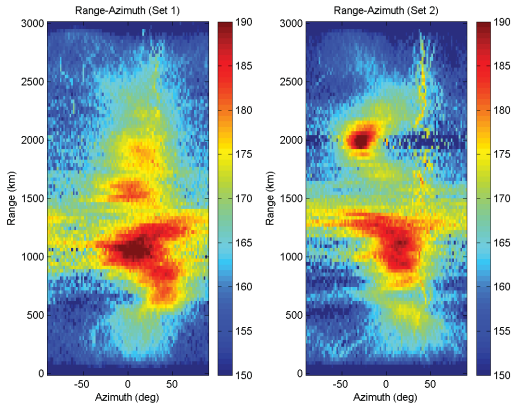

Fig. 3. Range-azimuth maps of Set 1 and Set 2.

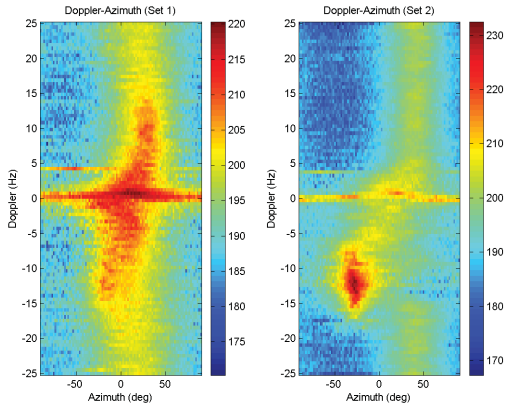

Fig. 4. Doppler-azimuth maps of Set 1 and Set 2.

for range bins near 2,000 km are dominated by the auroral clutter returns and thus other phase lags are suppressed. This effect is somewhat analogous to the so-called capture effect in FM reception, where only the stronger of two signals in the passband of the receiver is demodulated. We also note that an interference signal seen at about 40 degrees azimuth is similarly suppressed around 2,000 km.

Although the theory did not explicitly consider plasma motion, there is the possibility that plasma motion could produce an auroral clutter Doppler signature that could be exploited. Thus we examine the auroral clutter in Doppler-azimuth coordinates. In Figure 4 we see Doppler-azimuth processed results for Set 1 and Set 2, including all the data at ranges beyond 1,500 km. In Set 1, we see the ground clutter as a horizontal band near 0 Hz. An interference signal is seen at about 4 Hz, originating about -50 degrees in azimuth. The auroral clutter has some azimuth and Doppler dependence. At -15 Hz Doppler, the clutter is centered at about -20 degrees azimuth, whereas at 15 Hz Doppler, the clutter is centered at about 20 degrees azimuth. This phenomenon suggests that the clutter includes echoes from a rotating plasma convection pattern. The implication is that Space-Time Adaptive Processing (STAP) may be useful in this context to take advantage of the Doppler-azimuth coupling.

In Set 2, the auroral clutter is significantly localized in Doppler-azimuth, as might be expected by examination of the range-Doppler and range-azimuth maps. There is, however, a tail structure leading from the auroral clutter back to the coordinate origin that could be addressed through STAP. Also evident in this image is the ground clutter at 0 Hz, a narrowband interference signal at 4 Hz, and a broadband interference signal at around 40 degrees azimuth. The broadband interference was also seen in Figure 3. Furthermore, the capture effect is also visible in this figure in the manner in which the broadband source has been suppressed in the Doppler frequency range between -15 and -5 Hz. A more robust spectral estimator could be realized with a large beamforming array, perhaps in a shape of a cross in order to resolve both the azimuth and elevation extents with good resolution.

IV. Conclusion

Auroral clutter echoes have been resolved in three spatial dimensions by an OTHR system in Canada and a limited data set has been presented in this paper. The range-Doppler data suggest that the ground scene may sometimes be masked by the auroral clutter. The elevation distributions show that the auroral clutter echoes are confined to low elevation angles relative to the ground clutter, which suggests that the auroral clutter echoes could be reduced using spatial filtering with a 1-km endfire antenna array. Both the theory and experiment quantitatively show a slow rolloff in elevation, likely due to the effect of the PSF, which suggests that elevation filtering of the clutter should be performed on both transmit and receive to achieve adequate clutter suppression. Finally, the Doppler-azimuth data show joint Doppler-azimuth behavior that could be addressed using STAP methods.

References

[1] T. J. Elkins, "A model for high frequency radar auroral clutter," Rome Air Development Center, TR-80-122, 1980.

[2] J. M. Headrick, M. I. Skolnik, "Over-the-horizon radar in the HF band," *Proceedings of the IEEE*, vol. 62, no. 6, 664–673, 1974.

[3] J. M. Headrick, J. F. Thomason, "Applications of high-frequency radar," *Radio Science*, vol. 33, no. 4, 1045–1054, 1998.

[4] V. Bazin, J. P. Molinie, J. Munoz, P. Dorey, S. Saillant, G. Auffray, V. Rannou, M. Lesturgie, "NOSTRADAMUS: An OTH Radar," *IEEE Aerospace and Electronic Systems Magazine*, Vol. 21, no. 10, 3-11, 2006.

[5] X. Vallieres, J. P. Villain, C. Hanuise, R. Andre, "Ionospheric propagation effects on spectral widths measured by Superdarn HF radars," *Annales Geophysicae*, 22, 2023–2031, 1984.

[6] M. Ravan, R. J. Riddolls, R. S. Adve, "Ionospheric and auroral clutter models for HF surface wave and over the horizon radar systems," *Radio Science*, 47, doi: 10.1029/2011RS004944.

[7] R. J. Riddolls, "The three-dimensional spatial autocorrelation of ionospherically propagated wave packets in the Arctic region," *Proceedings of the IEEE Radar Conference*, 2013.

[8] R. J. Riddolls, "Hyperspace aperture concept for auroral clutter control in a Canadian over-the-horizon radar," *Proceedings of the IEEE Radar Conference*, 2012.

[9] J. M. Beall, Y. C. Kim, E.J. Powers, "Estimation of wavenumber and frequency spectra using fixed probe pairs," *Journal of Applied Physics*, Vol. 53, No. 6, 3933-3940.

[10] I. S. Reed. On a moment theorem for complex Gaussian processes. *IRE Transactions on Information Theory*, 8 (4), 194–195.

[11] M. Abramowitz, I. A. Stegun, *Handbook of mathematical functions with formulas, graphs, and mathematical tables*, New York: Dover., 1964,